Impurity effects of hyperons in hypernuclei with relativistic mean field theory in complex-momentum representation

Shu-Yuan Zhai, Tai-Hua Heng,* and Jian-You Guo†
School of Physics and Optoelectronic Engineering, Anhui University, Hefei 230601, China

(Received 20 May 2024; accepted 31 July 2024; published 19 August 2024)

Utilizing the recently formulated relativistic mean field theory in complex momentum representation, we delve into the impurity effects of hyperons in hypernuclei. Our findings reveal that hyperons exert considerable effects on single-neutron levels, particularly in the deeply bound states such as $1s$ and $1p$. In the case of $^{60}\mathrm{Ca}+\Lambda$, $^{60}\mathrm{Ca}+\Sigma^0$, $^{60}60+\Xi^0$, and $^{60}\mathrm{Ca}+\Sigma^+$, the neutron levels are noticeably lower compared to the baseline ^{60}Ca, indicating an increased neutron capacity and a shift in the neutron drip line. Notably, the introduction of Ξ^0 and Σ^+, especially Σ^+, hyperons results in a more pronounced reduction in neutron levels, partially attributed to the positive charge of the latter. Conversely, for $^{60}\mathrm{Ca}+\Sigma^-$ and $^{60}\mathrm{Ca}+\Xi^-$, the neutron levels are elevated, partly due to Coulomb attraction. The impurity effects of hyperons are further evidenced in their density distributions. Neutral Λ and Σ^0 hyperons exhibit similar patterns, but Coulomb effects notably alter the density distributions of Σ^+ and Σ^-. While Λ and Ξ^- possess comparable central densities, the diffuse distribution of Ξ^- hints at the formation of a hyperon halo. This study offers valuable insights into the intricate interactions between hyperons and nucleons within hypernuclei.

DOI: 10.1103/PhysRevC.110.024316

I. INTRODUCTION

Over the past decades, considerable attention has been devoted to the study of bound nuclear systems containing one or two hyperons ($Y = \Lambda$, Ξ, and Σ), which are baryons characterized by one or two strangeness quantum numbers (S). Since the pioneering discovery of the Λ hypernucleus by Danysz and Pniewski in 1953 [1], the realm of nuclear physics has been broadened to encompass the exploration of the strange degrees of freedom in atomic nuclei, as evidenced by both experimental [2–5] and theoretical [6] advancements. A key goal in hypernuclear research is to deepen our understanding of the baryon-baryon (BB) interaction, which is important for furthering our knowledge of nuclear structure [7–10] and for its applications in astrophysical settings [11–14].

The rapid advancement of radioactive nuclear beam facilities and detection technologies has led to significant strides in the experimental study of hypernuclei [15–19]. A diverse array of hypernuclear species have come into focus, categorized based on their strangeness quantum number. With $S = -1$, a multitude of bound single-Λ hypernuclei with various nuclear cores have been produced experimentally, ranging from the lightest $^3\mathrm{H}_\Lambda$ to the heaviest $^{208}\mathrm{Pb}_\Lambda$ [20,21]. In 1989, Hayano *et al.* [22] identified the first quasibound Σ hypernucleus, $^4\mathrm{He}_\Sigma$, which remains the sole recognized instance of a bound Σ hypernucleus to date. All double-Λ and single-Ξ hypernuclei hold the strangeness of $S = -2$. To date, only five double-Λ hypernuclei have been observed: $^6\mathrm{He}_{\Lambda\Lambda}$, $^{10}\mathrm{Be}_{\Lambda\Lambda}$, $^{13}\mathrm{B}_{\Lambda\Lambda}$, $^{12}\mathrm{Be}_{\Lambda\Lambda}$, and $^{11}\mathrm{Be}_{\Lambda\Lambda}$ [23–28].

Observations from the KEK-E377 experiment indicate a weak mutual attraction between Λ particles within the $^6\mathrm{He}_{\Lambda\Lambda}$ hypernucleus. Regarding single-Ξ hypernuclei, limited experimental data are available for $^{12}\mathrm{Be}_\Xi$ [29], $^{13}\mathrm{B}_\Xi$ [30], and $^{15}\mathrm{C}_\Xi$ [31]. Notably, the Kiso event involving $^{15}\mathrm{C}_\Xi$ provided the first definitive evidence of a deeply bound state in a $\Xi^- + {}^{14}\mathrm{N}$ system, facilitated by an attractive ΞN interaction. In the most recent experiment, the international collaborative laboratory RHIC-STAR pioneered the discovery of collective behavior in hypernuclear structures [32]. It is intriguing that while experimental research on hypernuclei continues to thrive, there is still a scarcity of data from hyperon-nucleon (YN) and hyperon-hyperon (YY) scattering experiments. Consequently, theoretical exploration of hypernuclear properties is crucial for furthering our understanding of nuclear physics.

The inclusion of an additional strangeness degree of freedom means that hyperons are not restricted by the Pauli exclusion principle within atomic nuclei. When a hyperon is incorporated into a nucleus, it penetrates deeply into the nuclear matter. Acting as an impurity, it can induce a variety of intriguing phenomena. Hypernuclear characteristics have been thoroughly investigated, including halo, skin, and bubble structures [33–37]. Moreover, the presence of hyperons has numerous effects on the nucleus, such as shifting the neutron drip line [38–40], causing deformation [41–45], cluster structure formation [46,47], shrinkage phenomenon [48], alterations in pseudospin symmetry [49,50], and more. Various theoretical methods have contributed to our understanding of hypernuclear properties. Among them, the G matrix is an effective method for dealing with many-body systems [51], and has been widely used in hypernuclear researches [52–56]. The Skyrme Hartree-Fock model represents one of the

*Contact author: hength@ahu.edu.cn
†Contact author: jianyou@ahu.edu.cn

nonrelativistic techniques suitable for dense environments exceeding nuclear saturation density yet far from stability [37,57,58]. Relativistic approaches provide an excellent description of hypernuclei, including the relativistic mean-field model [59,60], relativistic chiral effective field model [10,61], quark mean field model [62], among others.

Significant advancements have been made in the description of hypernuclear properties using relativistic mean-field (RMF) theory. Brockmann and Weise were pioneers in applying this theory to hypernuclei, successfully explaining the spin-orbit coupling phenomenon [63], which was consistent with experimental findings [64]. Various techniques are incorporated within RMF to study hypernuclear characteristics, such as the RMF theory with the point-coupling interactions [44] and the RMF theory integrated with Green's function approach [65].

Resonant states hold an irreplaceable role in the study of exotic nuclei, prompting the development of various methods to explore their significant properties. Based on the scattering theory, ones have developed the R-matrix method [66,67], the K-matrix method [68], the S-matrix method [69,70], and the scattering phase shift method [71,72]. Nevertheless, solving scattering problems can be exceedingly challenging. Alternative approaches have been proposed that are more akin to bound-state methods. These include the analytic continuation of the coupling constant method [73,74], the real stabilization method [75], the complex scaling method [76–79], and the complex momentum representation (CMR) method [80]. A notable advantage of the CMR method is its capability to simultaneously identify both narrow and broad resonant states.

Significant strides have been made by integrating the complex momentum method with relativistic mean field theory, leading to a synergistic approach that has proven fruitful in recent studies [81–85]. In this study, we expand the application of the Relativistic Mean Field-Complex Momentum Representation (RMF-CMR) method to explore the properties of hypernuclei. The comprehensive formulas for NN (nucleon-nucleon) and YN (hyperon-nucleon) interactions are elucidated. Using the stable nucleus ^{60}Ca as a core reference, we examine the impurity effects of Λ, Σ, and Ξ hyperons on the nuclear system. A detailed analysis is provided on how the inclusion of different hyperons affects the neutron single-particle levels, including those of resonant states. Furthermore, by considering isotopes of calcium (^{40,50,60}Ca), we investigate the impact of increasing neutron numbers on the mean-field potential and density distributions of hyperons. This work aims to deepen our understanding of hypernuclear structure and the role of strangeness in nuclear systems, paving the way for future experimental and theoretical advancements in the field of hypernuclear physics.

The paper is organized as follows. The RMF-CMR theory for the single-Λ, Ξ, and Σ hypernuclei is presented in Sec. II. The numerical results and discussions are given in Sec. III. A summary is provided in Sec. IV.

II. FORMALISM

To explore the impurity effects of hyperons in hypernuclei with the RMF-CMR theory, we briefly introduce the theoretical formalism. The Lagrange density for hypernuclei can be written as

$$\mathcal{L} = \mathcal{L}_N + \mathcal{L}_Y, \tag{1}$$

where $\mathcal{L}_N$ for nucleons is the same as that in Refs. [86–89], and will not be elaborated here. $\mathcal{L}_Y$ for hyperons is given as [59]

$$\begin{aligned}\mathcal{L}_Y =& \bar{\psi}_Y[i\gamma^\mu\partial_\mu - M_Y - g_{\sigma Y}\sigma - g_{\omega Y}\gamma^\mu\omega_\mu]\psi_Y \\ &+ \mathcal{L}_T + \mathcal{L}_{\rho Y} + \mathcal{L}_{AY},\end{aligned} \tag{2}$$

where $\mathcal{L}_T$ represents the ω-Y coupling

$$\mathcal{L}_T = \frac{f_{\omega Y}}{2M_Y}\bar{\psi}_Y\sigma^{\mu\nu}\partial_\nu\omega_\mu\psi_Y, \tag{3}$$

where M_Y is the mass of hyperon, and $g_{\sigma Y}$, $g_{\omega Y}$, and $g_{\rho Y}$ are the coupling coefficients with σ, ω, and ρ mesons. $f_{\omega Y}$ is the coefficient of the tensor coupling between hyperons and ω field.

The $\mathcal{L}_{\rho Y}$ and $\mathcal{L}_{AY}$ describe the interactions of hyperons with ρ meson and photons, respectively. For a particular hyperon, they can be expressed as

$$\mathcal{L}_{\rho Y} = \begin{cases} 0, & \text{for } \Lambda; \\ -\bar{\psi}_\Xi g_{\rho\Xi}\gamma^\mu\vec{\tau}_\Xi\cdot\vec{\rho}_\mu\psi_\Xi, & \text{for } \Xi; \\ -\bar{\psi}_\Sigma g_{\rho\Sigma}\gamma^\mu\vec{\tau}_\Sigma\cdot\vec{\rho}_\mu\psi_\Sigma, & \text{for } \Sigma, \end{cases} \tag{4}$$

$$\mathcal{L}_{AY} = \begin{cases} 0, & \text{for } \Lambda; \\ -\bar{\psi}_\Xi e\gamma^\mu\frac{\tau_{\Xi,3}-1}{2}A_\mu\psi_\Xi, & \text{for } \Xi; \\ -\bar{\psi}_\Sigma e\gamma^\mu\tau_{\Sigma,3}A_\mu\psi_\Sigma, & \text{for } \Sigma. \end{cases} \tag{5}$$

The $\vec{\tau}_Y$ is the isospin vector with the third component $\tau_{Y,3}$,

$$\tau_{Y,3} = \begin{cases} 0, & Y = \Lambda; \\ +1, -1, & Y = \Xi^0, \Xi^-; \\ +1, 0, -1, & Y = \Sigma^+, \Sigma^0, \Sigma^-. \end{cases} \tag{6}$$

For a static nucleus, only the time-like components ω^0, $\vec{\rho}^0$, and A^0 are reserved. The charge conservation guarantees that only the three-components of the isovector $\rho_{0,3}$ exist. For the NN interactions, the PK1 parameter is adopted. For the YN interactions, the adopted coupling coefficients are same as those in Refs. [50,59,90], i.e., $g_{\sigma Y} = \alpha_{\sigma Y}g_{\sigma N}$, $g_{\omega Y} = \alpha_{\omega Y}g_{\omega N}$, $g_{\rho Y} = \alpha_{\rho Y}g_{\rho N}$, and $f_{\omega Y} = \alpha_{TY}g_{\omega Y}$.

Based on the Lagrange density, the Dirac equation describing baryons is obtained as

$$[\vec{\alpha}\cdot\vec{p} + V(\vec{r}) + \beta(M_B + S(\vec{r})) + T(\vec{r})]\psi_i(\vec{r}) = \varepsilon_i\psi_i(\vec{r}), \tag{7}$$

where M_B is the mass of the baryons, $\vec{\alpha}$ and β are the Dirac matrix. The scalar potential $S(\vec{r})$, vector potential $V(\vec{r})$, and tensor potential $T(\vec{r})$ are

$$S(\vec{r}) = \begin{cases} g_\sigma\sigma(\vec{r}), & \text{for nucleons} \\ g_{\sigma Y}\sigma(\vec{r}), & \text{for } \Lambda, \Xi, \Sigma \end{cases}, \tag{8}$$

$$V(\vec{r}) = \begin{cases} g_\omega \omega_0(\vec{r}) + g_\rho \tau_3 \rho_0(\vec{r}) + eA_0(\vec{r}), & \text{for } N \\ g_{\omega\Lambda}\omega_0(\vec{r}), & \text{for } \Lambda \\ g_{\omega\Xi}\omega_0(\vec{r}) + g_{\rho\Xi}\tau_{\Xi,3}\rho_{0,3}(\vec{r}) + \frac{\tau_{\Xi,3}-1}{2} eA_0(\vec{r}), & \text{for } \Xi \\ g_{\omega\Sigma}\omega_0(\vec{r}) + g_{\rho\Sigma}\tau_{\Sigma,3}\rho_{0,3}(\vec{r}) + e\tau_{\Sigma,3}A_0(\vec{r}), & \text{for } \Sigma \end{cases}, \tag{9}$$

$$T(\vec{r}) = -\beta(\vec{\alpha}\cdot\vec{p})V_T(\vec{r}) + V_T(\vec{r})\beta(\vec{\alpha}\cdot\vec{p}). \tag{10}$$

Correspondingly, the radial meson and photon field equation are expressed as

$$\left(-\frac{d^2}{dr^2} - \frac{2}{r}\frac{d}{dr}\right)\phi = S_\phi \tag{11}$$

with the source terms

$$S_\phi = \begin{cases} -m_\sigma^2\sigma - g_\sigma\rho_s - g_{\sigma Y}\rho_{sY} - g_2\sigma^2 - g_3\sigma^3, \\ -m_\omega^2\omega + g_\omega\rho_v + g_{\omega Y}\rho_{vY} + \frac{f_{\omega Y}}{2M_Y}\partial_i j_{TY}^{0i} - c_3\omega^3, \\ -m_\rho^2\rho_{0,3} + g_\rho\rho_3 + g_{\rho Y}\rho_{3Y}, \\ +e\rho_c + e\rho_{cY}, \end{cases} \tag{12}$$

where $m_{(\sigma,\omega,\rho)}$ is the meson mass. $g_{(\sigma,\omega,\rho)}$, $g_{(2,3)}$, and c_3 are the parameters for the NN interactions, $\rho_s(\rho_{sY})$, $\rho_v(\rho_{vY})$, $\rho_3(\rho_{3Y})$, and $\rho_c(\rho_{cY})$ are the scalar, baryon, isovector, and charge density densities for the nucleons (hyperons). j_{TY}^{0i} is the tensor density for the hyperons.

The densities for hyperons can be expressed as

$$\rho_{sY}(r) = \sum_{i=1}^{A_Y}[f^*(r)f(r) - g^*(r)g(r)],$$

$$\rho_{vY}(r) = \sum_{i=1}^{A_Y}[f^*(r)f(r) + g^*(r)g(r)],$$

$$j_{TY}^{0i}(r) = \sum_{i=1}^{A_Y}[f^*(r)g(r) + g^*(r)f(r)]\boldsymbol{n},$$

$$\rho_{3Y}^{0}(r) = \sum_{i=1}^{A_Y}[f^*(r)f(r) + g^*(r)g(r)]\tau_{Y,3},$$

$$\rho_{cY}(r) = \begin{cases} \sum_{i=1}^{A_Y}[f^*(r)f(r) + g^*(r)g(r)]\frac{\tau_{\Xi,3}-1}{2}, & \text{for } \Xi \\ \sum_{i=1}^{A_Y}[f^*(r)f(r) + g^*(r)g(r)]\tau_{\Sigma,3}, & \text{for } \Sigma \end{cases},$$

where n is the unit vector.

The hyperon number A_Y is determined by the baryon density $\rho_{vY}(r)$ as

$$A_Y = \int r^2 dr \rho_{vY}(r).$$

For hypernuclei, the total baryon (mass) number A is the summation of the neutron, proton, and hyperon numbers.

To include the resonant states, the Dirac equation is transformed into the complex momentum space

$$\int d\vec{k}'\langle\vec{k}|H|\vec{k}'\rangle = \varepsilon\psi(\vec{k}), \tag{13}$$

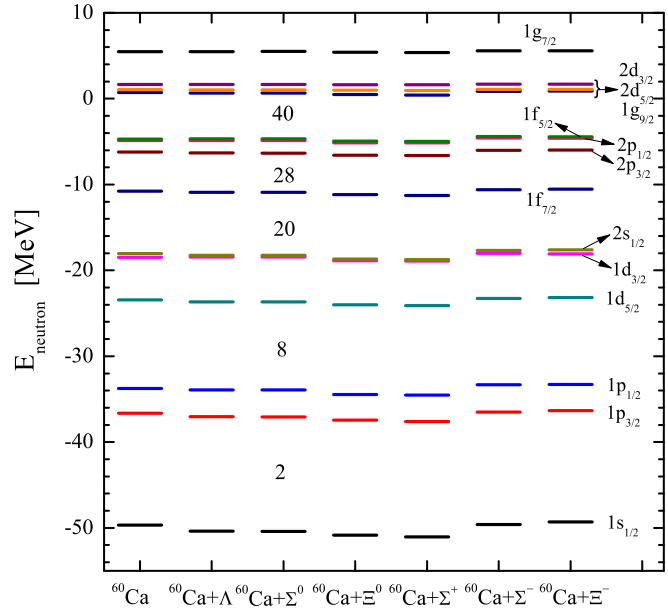

FIG. 1. The calculated single-particle energy levels for neutrons in ^{60}Ca and ^{60}Ca $+Y$ ($Y = \Lambda$, $\Xi^{0,-}$, $\Sigma^{+,0,-}$), wherein the bound and resonant levels are demarcated by solid lines of varying colors. The states are designated by the notation nl_j with n representing the radial quantum number, l the orbital angular momentum quantum number, and j the total angular momentum quantum number.

where H is the Dirac Hamiltonian and $\vec{k} = \vec{p}/\hbar$ is the wave vector. In the spherical case,

$$\psi(\vec{k}) = \begin{pmatrix} f(k)\Phi_{ljm_j}(\Omega_k) \\ g(k)\Phi_{\tilde{l}jm_j}(\Omega_k) \end{pmatrix}. \tag{14}$$

The upper and lower components of the Dirac spinor in the coordinate space can be calculated by the following formulas:

$$f(r) = i^l\sqrt{\frac{2}{\pi}}\int k^2 dk j_l(kr)f(k),$$

$$g(r) = i^{\tilde{l}}\sqrt{\frac{2}{\pi}}\int k^2 dk j_{\tilde{l}}(kr)g(k). \tag{15}$$

In the RMF-CMR formalism, the coupled equations (7)–(15) are solved numerically for hyperons accompanying consistent solutions with Ref. [81] for nucleons.

III. RESULTS AND DISCUSSIONS

Based on our developed RMF-CMR formalism, which is particularly appropriate for the unified description of stable nuclei and weakly bound exotic nuclei, we explore the impurity effects of hyperons in hypernuclei. Without losing generality, we chose ^{60}Ca $+Y$ (often instead of $^{61}_{Y}$Ca) hypernuclei as an example for study, and the corresponding impurities include the Λ, Ξ, and Σ hyperons.

We first examine the effect of the introduction of hyperons on the single-particle levels of nucleons. The effects of different hyperons on the neutron levels in the ^{60}Ca $+Y$ are plotted in Fig. 1. For comparison, the single neutron levels

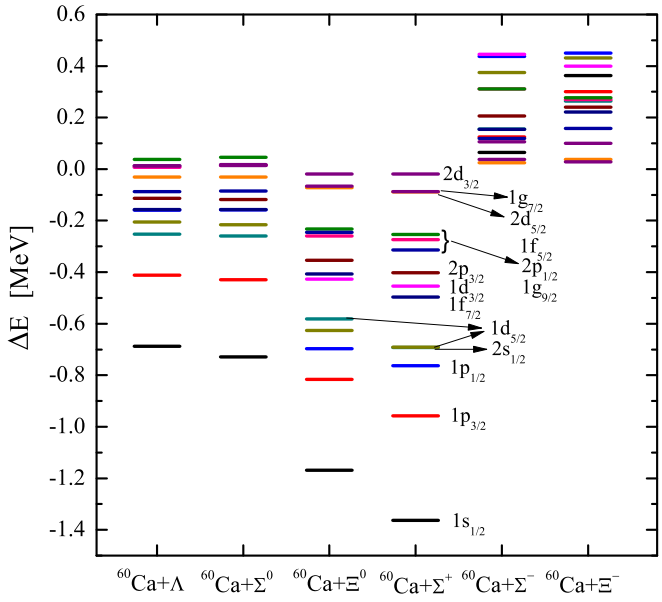

FIG. 2. The energy difference ΔE of the neutron levels between ^{60}Ca $+Y$ and ^{60}Ca ($Y = \Lambda, \Xi^{0,-}, \Sigma^{+,0,-}$). The energy difference for each energy level is marked with a solid line of the same color as in Fig. 1.

in ^{60}Ca without the introduction of hyperons are also plotted there. Overall, the introduction of hyperons in hypernuclei has a non-negligible impact on the neutron levels in hypernuclei ^{60}Ca $+Y$. The energies of neutron levels in some hypernuclei increases, while the energies of neutron levels decreases in others. Comparatively, the more bound the level, the more significantly affected by hyperons. For the resonant levels, their energies are weakly affected by the hyperons especially those in the vicinity of the Fermi surface. In addition, we have also observed that for almost all the neutron levels, the influence of the Σ^+ hyperon is significant. Although hyperons have an important influence on the neutron levels in the hypernuclei, this influence is not enough to change the shell structure of the neutron levels, and the traditional magic number is still clearly displayed in the neutron single particle levels as shown in Fig. 1.

Since the influence of hyperons on the neutron energy levels within the hypernuclei is not particularly pronounced, to distinctly illustrate this effect, we have extracted the energy differences of the neutron levels between ^{60}Ca $+Y$ and ^{60}Ca. This comparison is depicted in Fig. 2 for clarity. For the hypernuclear systems ^{60}Ca $+\Lambda$, ^{60}Ca $+\Sigma^0$, ^{60}Ca $+\Xi^0$, and ^{60}Ca $+\Sigma^+$, the energy differences of the neutron levels between these hypernuclei and the standard ^{60}60 are predominantly negative across nearly all energy levels. This indicates that the incorporation of a hyperon into the nucleus facilitates an increased neutron capacity within the nuclear structure. In comparison to ^{60}Ca $+\Lambda$ and ^{60}Ca $+\Sigma^0$, the addition of a hyperon to form ^{60}Ca $+\Xi^0$ and ^{60}Ca $+\Sigma^+$ results in a more pronounced decrease in neutron levels, implying a stronger binding of neutrons. Consequently, these hypernuclei can sustain a larger neutron population, leading to a shift in the neutron dripline towards regions with higher neutron abundance, particularly notable in the case of ^{60}Ca $+\Sigma^+$. Moreover, our observations revealed that the most significant energy differences of the neutron levels between the hypernuclei ^{60}Ca $+Y$ and the base ^{60}Ca occurs at the deeply bound $1s$ orbital, followed by the $1p$ orbital, with the $1s$ level exhibiting an energy difference nearly twice that of the $1p$ level. This suggests that the inclusion of hyperons has a more substantial impact on the binding of deeply bound neutrons within the energy spectrum. Among the hyperons considered, the Σ^+ yields the most considerable reduction in neutron energy levels within the hypernucleus, potentially attributable, in part, to the contribution of its positive charge.

TABLE I. The energies $\varepsilon_{\rm res}$ and widths τ with unit MeV for the single-neutron resonant states in ^{60}Ca and ^{60}Ca $+Y$ ($Y = \Lambda, \Xi^{0,-}, \Sigma^{+,0,-}$).

		$1g_{9/2}$	$2d_{5/2}$	$2d_{3/2}$	$1g_{7/2}$
^{60}Ca	$\varepsilon_{\rm res}$	0.7283	1.0496	1.6467	5.1793
	τ	0.0003	0.5886	1.8269	1.1209
^{60}Ca $+\Lambda$	$\varepsilon_{\rm res}$	0.6399	1.0163	1.6590	5.4925
	τ	0.0002	0.5495	1.8684	1.1320
^{60}Ca $+\Sigma^0$	$\varepsilon_{\rm res}$	0.6439	1.0160	1.6610	5.4973
	τ	0.0002	0.5489	1.8753	1.1352
^{60}Ca $+\Xi^0$	$\varepsilon_{\rm res}$	0.4832	0.9748	1.6279	5.4126
	τ	0.0001	0.4938	1.7323	1.0557
^{60}Ca $+\Sigma^-$	$\varepsilon_{\rm res}$	0.8477	1.0721	1.6848	5.5853
	τ	0.0006	0.6292	2.0064	1.2209
^{60}Ca $+\Xi^-$	$\varepsilon_{\rm res}$	0.8855	1.0845	1.6750	5.5788
	τ	0.0008	0.6460	1.9651	1.2135
^{60}Ca $+\Sigma^+$	$\varepsilon_{\rm res}$	0.4143	0.9583	1.6276	5.3924
	τ	0.00003	0.4753	1.7327	1.0440

Distinct from the aforementioned four hypernuclear species, the energy differences of the neutron levels between ^{60}Ca $+Y$ and ^{60}Ca for ^{60}Ca $+\Sigma^-$ and ^{60}Ca $+\Xi^-$ are consistently positive. This phenomenon arises partly from the fact that these hyperons carry a negative charge. Consequently, the electrostatic interactions between the negatively charged hyperons and the positively charged protons within the nucleus intensify the binding of the protons. This increased proton binding energy results in an elevation of the neutron energy levels, leading to a scenario where the neutron energy levels become excessively high relative to the proton energy levels.

The incorporation of hyperons into hypernuclei modulates the neutron energy levels, with the most pronounced effects observed in the deeply bound energy levels, as evidenced by Figs. 1 and 2. To elucidate the influence of hyperon introduction on neutron resonance energy levels, we have compiled the resonant state energies $\varepsilon_{\rm res}$ and widths τ for neutrons in ^{60}Ca $+Y$ in Table I. Across all these resonance levels, the presence of hyperons either amplifies or diminishes the energy and width of these levels. The most substantial disparity in neutron energy levels between ^{60}Ca $+Y$ and ^{60}Ca manifests in the $1g$ state for ^{60}Ca $+\Sigma^+$, where the difference approximates 0.3 MeV and 0.1 MeV, respectively. This indicates that the inclusion of hyperons alters both the positioning and the lifetime

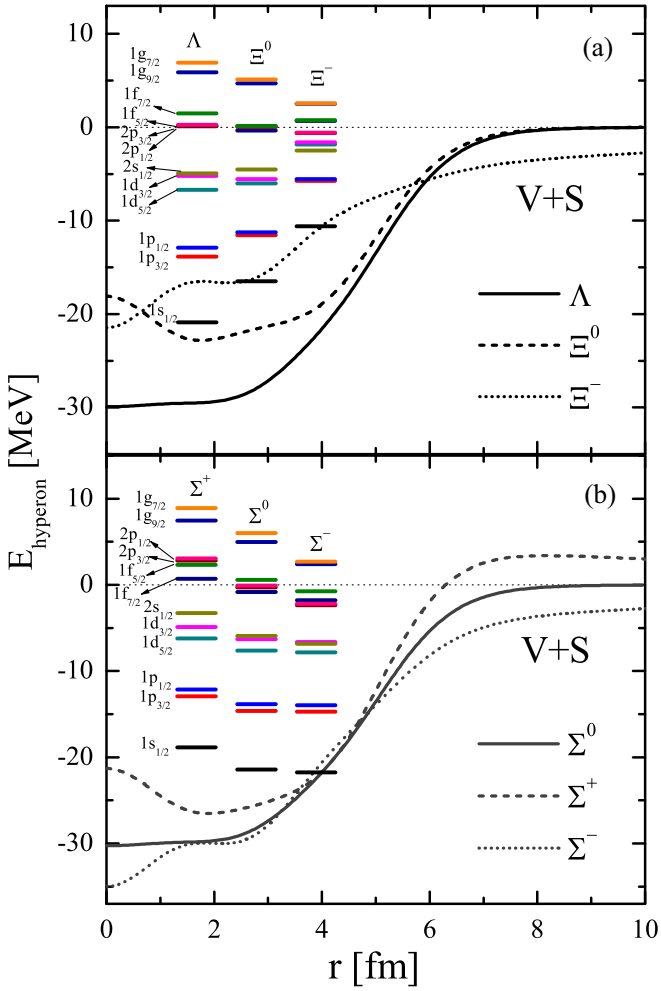

FIG. 3. Mean-field potentials $V + S$ and single-hyperon levels for the hyperons in the hypernuclei ^{60}Ca +Y ($Y = \Lambda$, $\Xi^{0,-}$, $\Sigma^{+,0,-}$).

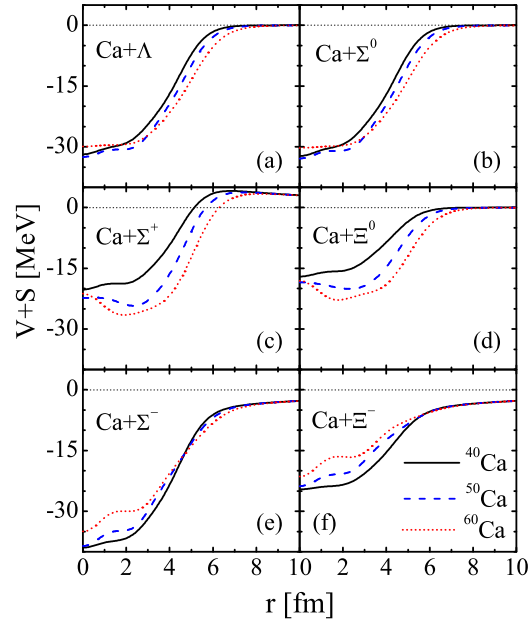

FIG. 4. The Mean-field potentials $V + S$ for the hyperons Λ, $\Xi^{0,-}$, and $\Sigma^{+,0,-}$ in nuclear core ^{40}Ca, ^{50}Ca, and ^{60}Ca.

of neutron resonance states. These findings underscore that the perturbative effect of hyperons is significant and cannot be overlooked, whether considering bound states or resonance states.

To understand why different hyperons cause different impurity effects, we compare the differences in the single-particle energy levels of hyperons and the corresponding potential of hyperon in hypernuclei. The single-hyperon levels accompanying corresponding potential of hyperon in hypernuclei $^{60}60+Y$ are plotted in Fig. 3. In Figs. 3(a) and 3(b), the mean-field potentials $V + S$ for Λ and Σ^0 hyperons are very similar, which is owing to the fact that Λ and Σ^0 hyperons have the same quark combination—**uds**. However, they are only coupled with σ and ω mesons and have almost the same coupling coefficients ($\alpha_{\sigma\Lambda} = 0.618$, $\alpha_{\omega\Lambda} = 0.667$, $\alpha_{\sigma\Sigma} = 0.619$, and $\alpha_{\omega\Sigma} = 0.667$). The central part of the potentials of Ξ^0 hyperon is about 12 MeV shallower than that of Λ and Σ^0 hyperons, which is mainly because the couplings of $\sigma - \Xi^0$ and $\omega - \Xi^0$ ($\alpha_{\sigma\Xi^0} = 0.313$, $\alpha_{\omega\Xi^0} = 0.333$) are about half of those for $\sigma - \Lambda$ and $\omega - \Lambda$. Compared with Λ and Σ^0 hyperons, the mean-field potentials $V + S$ for Σ^- hyperons is more deep. The corresponding energy levels of Σ^- hyperons are more bound. While the mean-field potentials $V + S$ for the Ξ^0 hyperon is relatively more shallow, the corresponding energy levels of Ξ^0 hyperons are weakly bound. However for the Ξ^- hyperon, its hyperon potential is shallower, but the potential expands to a larger range. Different from the previous hyperon potentials, there is a Coulomb barrier in the mean-field potentials $V + S$ for Σ^+ hyperons.

Since there are significant differences in these hyperonic potentials, this results in a large difference in the corresponding hyperonic energy levels. Despite this, the single-particle energy levels of all hyperons have a shell structure similar to that of neutrons and protons with magic numbers 2, 8, 20 appearing. It is evident that the spin-orbit splittings of the Ξ^0, Ξ^-, and Σ^- hyperons are exceedingly small when the tensor potential is not taken into account. The spin-orbit splitting energies of the other three hyperons are also all less than 1.5 MeV. Furthermore, the spin-orbit splittings between the spin doublet states p, d, f, and g are substantially smaller than those observed for neutrons, as illustrated in Fig. 1. In line with experimental observations, the spin-orbit coupling in the Λ-nucleon interaction is at least an order of magnitude smaller than that in the nucleon-nucleon interaction, as cited in Refs. [64,91].

The impurity effects of different hyperons in ^{60}Ca nuclei have been discussed earlier. Whether this effect is related to the neutron and proton potential fields of the nucleus. In order to make it clear, in Fig. 4, we have plotted the mean field potentials $V + S$ of the hyperons in Ca isotopes with nucleon numbers 40, 50, and 60. The potentials of hyperons change differently with the increase of neutrons. For the Λ and Σ^0 hyperons in Figs. 4(a) and 4(b), the depth and shape of the potentials do not change much with the nuclear core ^{40}Ca, ^{50}50, and ^{60}Ca, because both Λ and Σ^0 are electroneutral and the isospin third component $\tau_{Y,3} = 0$. Compared to

Λ and Σ^0, the evolution of the potentials of Ξ^0 hyperon is obvious in Fig. 4(d). Although Ξ^0 is also electroneutral, the couplings strength of $\sigma(\omega) - \Xi^0$ is weaker than that of $\sigma(\omega) - \Lambda$. There is a significant change in the potentials of Ξ^0 as the nuclear core potentials becomes deeper from ^{40}Ca to ^{60}Ca. The coupling strength of the meson-hyperon has a meaningful influence on the hypernuclei systems. Comparing the potentials of Σ^0, Σ^+, and Σ^- in Figs. 4(b), 4(c), and 4(e), the potentials of Σ^+ and Σ^- hyperons change significantly with the increase of neutrons. The factor is partly the charge of the hyperon. Because of the repulsive Coulomb interaction, the central part of mean-field potential for Σ^+ is higher than that of Σ^0. Similarly, for Σ^+ and Σ^- hypernuclei, the center of potentials becomes deeper by almost 15 MeV, which illustrates that the charge interaction has a considerable effect on the hypernuclear system. Obviously, the Coulomb barriers are around 4 MeV near the nuclear surface of the Σ^+ hyperon. As the number of neutron increases, the Σ^+ hyperon becomes more bound while the Σ^- does the opposite. This is presumably because the (attractive or repulsive) Coulomb interaction is counterbalanced by the increased YN interaction. The potential of Ξ^- evolves for the same reason. Compared to the Ξ^0 hyperon, the potential for the negatively charged Ξ^- hyperon in Fig. 4(f). With the $Z = N$ nucleus ^{40}Ca as the core, the potential of the negatively charged hyperon Ξ^- is much deeper than that of the electroneutral hyperon Ξ^0. However, in the ^{60}Ca nucleus, the behavior is opposite. The same situation occurs for $\Sigma^{+,0,-}$ hyperons. This is because the enhanced YN interaction is much stronger than the charge interaction as the number of neutrons increases. That is why the depths of the potentials for Σ^0 and Σ^- are so close for the ^{60}Ca core in Fig. 3(b).

To further understand the impurity effects of hyperons in hypernuclei, we compare the density distributions of different hyperons in hypernuclei. The density distributions $\rho_v(r)$ for hyperons in ^{60}Ca $+Y$ systems are plotted in Fig. 5. That for $Y = \Lambda, \Xi^0$, and Ξ^- are placed on the top panel of Fig. 5 and that for $Y = \Sigma^+, \Sigma^0$, and Σ^- on the bottom panel. Only ground-state hypernuclei are considered here, the single-hyperon occupies $1s_{1/2}$ orbit. For ^{60}Ca $+\Lambda$ and ^{60}Ca $+\Sigma^0$ hypernuclei, since the single-hyperon energies of the $1s_{1/2}$ levels are almost the same, the density distributions of Λ in ^{60}Ca $+\Lambda$ and Σ^0 hyperons in ^{60}Ca $+\Sigma^0$ are very similar. For $^{60}60 + \Sigma^+$ and ^{60}Ca $+\Sigma^-$, due to the Coulomb interaction, the central density of the positively charged Σ^+ hyperon is depressed, while the central density of the negatively charged Σ^- hyperon is raised. For Λ and Ξ^- hyperons, their central densities are very similar, but the density of Ξ^- hyperons is more diffuse, which is due to the shallowest Ξ^- hyperon potential as shown in Fig. 3. The hyperon halo is most likely to be formed in the ^{60}Ca $+\Xi^-$ hypernucleus.

IV. SUMMARY

Based on our developed RMF-CMR framework, we investigate the impurity effects of hyperons in hypernuclei, specifically using ^{60}Ca $+Y$ (often serving as a surrogate for $^{61}_{Y}$Ca) as an illustrative case. The impurities considered include the Λ, Ξ, and Σ hyperons. Our initial examination

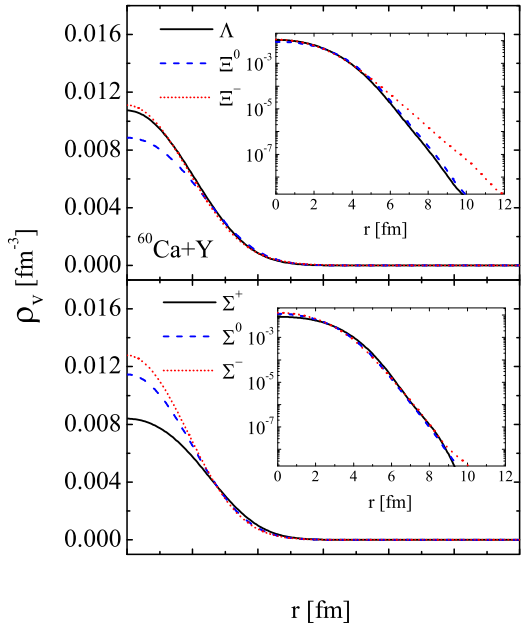

FIG. 5. Density distributions ρ_v for the hyperons in the hypernuclei ^{60}Ca $+$Y. In the top panel, Y $= \Lambda$ and $\Xi^{0,-}$; in the bottom panel, Y $= \Sigma^{+,0,-}$. The inserted figures are the same, but the ordinate is in the form of a logarithm based on 10.

focuses on the impact of hyperon introduction on the single-particle energy levels of nucleons. In hypernuclei such as ^{60}Ca $+Y$, the introduction of hyperons exerts a non-negligible influence on the neutron energy levels, with the more tightly bound levels experiencing more significant effects. For resonant levels, however, their energies are weakly perturbed by the presence of hyperons. Notably, the Σ^+ hyperon has a substantial impact. Although the neutron energy levels in these hypernuclei are affected by the hyperons, the effect is not significant enough to alter the shell structure of the neutrons.

For the hypernuclear systems ^{60}Ca $+\Lambda$, ^{60}Ca $+\Sigma^0$, ^{60}Ca $+\Xi^0$, and ^{60}Ca $+\Sigma^+$, the differences in neutron energy levels between these hypernuclei and the baseline ^{60}Ca nucleus are predominantly negative across a wide range of energy levels. This indicates that the incorporation of a hyperon into the nucleus facilitates an enhanced neutron capacity within the nuclear structure. Compared to $^{60}60 + \Lambda$ and ^{60}Ca $+\Sigma^0$, the addition of a hyperon to form ^{60}Ca $+\Xi^0$ and ^{60}Ca $+\Sigma^+$ results in a more pronounced decrease in neutron energy levels, suggesting a stronger binding of neutrons.

The most significant neutron energy level differences between the hypernuclei ^{60}Ca $+Y$ and the baseline ^{60}Ca occur in the deeply bound $1s$ orbital, followed by the $1p$ orbital. Among the hyperons considered, the Σ^+ hyperon yields the most considerable reduction in neutron energy levels within the hypernucleus, potentially attributed, in part, to its positive charge.

In the case of ^{60}Ca $+\Sigma^-$, given that Σ^- carries a negative charge, it may experience Coulomb attraction with protons within the nucleus. This could lead to a contrasting trend in neutron energy levels compared to hyperons with positive charges, such as Σ^+. However, the specific energy level

differences and the underlying mechanisms require further investigation and calculations for confirmation.

To understand hyperon impurity effects in hypernuclei, we compare density distributions of various hyperons. For neutral hyperons Λ and Σ^0 in ^{60}Ca $+\Lambda$ and ^{60}Ca $+\Sigma^0$, similar distributions are observed due to similar single-hyperon energies. However, Coulomb interactions cause the positively charged Σ^+ in ^{60}Ca $+\Sigma^+$ to have a depressed central density, while the negatively charged Σ^- in ^{60}Ca $+\Sigma^-$ exhibits an elevated central density. Λ and Ξ^- hyperons have similar central densities, but the Ξ^- density distribution in ^{60}Ca $+\Xi^-$ is more diffuse due to its shallower potential, suggesting a higher likelihood of forming a hyperon halo.

In summary, our study reveals significant effects of hyperons on neutron energy levels in hypernuclei, particularly the Σ^+ hyperon. These findings are important for understanding the structure and properties of hypernuclei and provide valuable insights for future experimental and theoretical research.

ACKNOWLEDGMENTS

This work was partly supported by the National Natural Science Foundation of China under Grants No. 11935001 and No. 11575002, the Natural Science Foundation of Anhui Province under Grant No. 2008085MA26, Anhui project (Project No. Z010118169), Heavy Ion Research Facility in Lanzhou (HIRFL) (Project No. HIR2021PY007), the project of Key Laboratory of High Precision Nuclear Spectroscopy in Chinese Academy of Sciences, Graduate Scientific Research Project of Anhui University (Project No. YJ20210096).

[1] M. Danysz and J. Pniewski, Philos. Mag. **44**, 348 (1953).
[2] O. Hashimoto and H. Tamura, Prog. Part. Nucl. Phys. **57**, 564 (2006).
[3] A. Feliciello and T. Nagae, Rep. Prog. Phys. **78**, 096301 (2015).
[4] T. R. Saito, W. Dou, V. Drozd, H. Ekawa, S. Escrig, Y. He, N. Kalantar-Nayestanaki, A. Kasagi, M. Kavatsyuk, E. Liu *et al.*, Nat. Rev. Phys. **3**, 803 (2021).
[5] T. Nagae, Prog. Theor. Phys. Suppl. **185**, 299 (2010).
[6] A. Gal, E. V. Hungerford, and D. J. Millener, Rev. Mod. Phys. **88**, 035004 (2016).
[7] J. Hao, T. T. S. Kuo, A. Reuber, K. Holinde, J. Speth, and D. J. Millener, Phys. Rev. Lett. **71**, 1498 (1993).
[8] E. Hiyama, T. Motoba, T. A. Rijken, and Y. Yamamoto, Prog. Theor. Phys. Suppl. **185**, 1 (2010).
[9] Y.-T. Rong, P. Zhao, and S.-G. Zhou, Phys. Lett. B **807**, 135533 (2020).
[10] Z.-W. Liu, J. Song, K.-W. Li, and L.-S. Geng, Phys. Rev. C **103**, 025201 (2021).
[11] J. Schaffner-Bielich, Nucl. Phys. A **804**, 309 (2008).
[12] I. Vidaña, Nucl. Phys. A **914**, 367 (2013).
[13] M. Fortin, S. S. Avancini, C. Providencia, and I. Vidana, Phys. Rev. C **95**, 065803 (2017).
[14] Y. Zhang, J. N. Hu, and P. Liu, Phys. Rev. C **97**, 015805 (2018).
[15] S. Okada, S. Ajimura, K. Aoki, A. Banu, H. C. Bhang, T. Fukuda, O. Hashimoto, J. I. Hwang, S. Kameoka, B. H. Kang *et al.*, Phys. Lett. B **597**, 249 (2004).
[16] E. Botta, T. Bressani, and G. Garbarino, Eur. Phys. J. A **48**, 41 (2012).
[17] H. Ohnishi, F. Sakuma, and T. Takahashi, Prog. Part. Nucl. Phys. **113**, 103773 (2020).
[18] S. H. Hayakawa, K. Agari, J. K. Ahn, T. Akaishi, Y. Akazawa, S. Ashikaga, B. Bassalleck, S. Bleser, H. Ekawa, Y. Endo *et al.* (J-PARC E07 Collaboration), Phys. Rev. Lett. **126**, 062501 (2021).
[19] T. R. Saito, H. Ekawa, and M. Nakagawa, Eur. Phys. J. A **57**, 159 (2021).
[20] H. Hotchi, T. Nagae, H. Outa, H. Noumi, M. Sekimoto, T. Fukuda, H. Bhang, Y. D. Kim, J. H. Kim, H. Park *et al.*, Phys. Rev. C **64**, 044302 (2001).
[21] F. Garibaldi, O. Hashimoto, J. J. LeRose, P. Markowitz, S. N. Nakamura, J. Reinhold, and L. Tang, J. Phys.: Conf. Ser. **299**, 012013 (2011).
[22] R. S. Hayano, T. Ishikawa, M. Iwasaki, H. Outa, E. Takada, H. Tamura, A. Sakaguchi, M. Aoki, and T. Yamazaki, Phys. Lett. B **231**, 355 (1989).
[23] D. J. Prowse, Phys. Rev. Lett. **17**, 782 (1966).
[24] H. Takahashi, J. K. Ahn, H. Akikawa, S. Aoki, K. Arai, S. Y. Bahk, K. M. Baik, B. Bassalleck, J. H. Chung, M. S. Chung *et al.*, Phys. Rev. Lett. **87**, 212502 (2001).
[25] J. K. Ahn, H. Akikawa, S. Aoki, K. Arai, S. Y. Bahk, K. M. Baik, B. Bassalleck, J. H. Chung, M. S. Chung, D. H. Davis *et al.* (E373 (KEK-PS) Collaboration), Phys. Rev. C **88**, 014003 (2013).
[26] M. Danysz, K. Garbowska, J. Pniewski, T. Pniewski, J. Zakrzewski, E. R. Fletcher, J. Lemonne, P. Renard, J. Sacton, W. T. Toner *et al.*, Nucl. Phys. **49**, 121 (1963).
[27] S. Aoki, S. Y. Bahk, K. S. Chung, S. H. Chung, H. Funahashi, C. H. Hahn, T. Hara, S. Hirata, K. Hoshino, M. Ieiri *et al.*, Prog. Theor. Phys. **85**, 1287 (1991).
[28] H. Ekawa, K. Agari, J. K. Ahn, T. Akaishi, Y. Akazawa, S. Ashikaga, B. Bassalleck, S. Bleser, Y. Endo, Y. Fujikawa *et al.*, Prog. Theor. Exp. Phys. **2019**, 021D02 (2019).
[29] P. Khaustov, D. E. Alburger, P. D. Barnes, B. Bassalleck, A. R. Berdoz, A. Biglan, T. Bürger, D. S. Carman, R. E. Chrien, C. A. Davi *et al.* (The AGS E885 Collaboration), Phys. Rev. C **61**, 054603 (2000).
[30] S. Aoki, S. Y. Bahk, K. S. Chung, S. H. Chung, H. Funahashi, C. H. Hahn, T. Hara, S. Hirata, K. Hoshino, M. Ieiri *et al.*, Prog. Theor. Phys. **89**, 493 (1993).
[31] K. Nakazawa, Y. Endo, S. Fukunaga, K. Hoshino, S. H. Hwang, K. Imai, H. Ito, K. Itonaga, T. Kanda, M. Kawasaki *et al.*, Prog. Theor. Exp. Phys. **2015**, 33D02 (2015).
[32] B. E. Aboona, J. Adam, J. R. Adams, G. Agakishiev, I. Aggarwal, M. M. Aggarwal, Z. Ahammed, A. Aitbaev, I. Alekseev, D. M. Anderson *et al.* (STAR Collaboration), Phys. Rev. Lett. **130**, 212301 (2023).
[33] E. Hiyama, M. Kamimura, T. Motoba, T. Yamada, and Y. Yamamoto, Phys. Rev. C **53**, 2075 (1996).
[34] H. F. Lü and J. Meng, Chin. Phys. Lett. **19**, 1775 (2002).
[35] H. F. Lü, J. Meng, S. Q. Zhang, and S. G. Zhou, Eur. Phys. J. A **17**, 19 (2003).
[36] E. Khan, J. Margueron, F. Gulminelli, and Ad. R. Raduta, Phys. Rev. C **92**, 044313 (2015).

[37] Y. Zhang, H. Sagawa, and E. Hiyama, Phys. Rev. C **103**, 034321 (2021).
[38] D. Vretenar, W. Poschl, G. A. Lalazissis, and P. Ring, Phys. Rev. C **57**, R1060 (1998).
[39] X. R. Zhou, A. Polls, H. J. Schulze, and I. Vidaña, Phys. Rev. C **78**, 054306 (2008).
[40] N. Buyukcizmeci, A. S. Botvina, J. Pochodzalla, and M. Bleicher, Phys. Rev. C **88**, 014611 (2013).
[41] J. Žofka, Czech. J. Phys. B **30**, 95 (1980).
[42] X. R. Zhou, H.-J. Schulze, H. Sagawa, C.-X. Wu, and E.-G. Zhao, Phys. Rev. C **76**, 034312 (2007).
[43] M. T. Win and K. Hagino, Phys. Rev. C **78**, 054311 (2008).
[44] X. Y. Wu, H. Mei, J. M. Yao, and X. R. Zhou, Phys. Rev. C **95**, 034309 (2017).
[45] C. Chen, Q.-K. Sun, Y.-X. Li, and T.-T. Sun, Sci. China Phys. Mech. Astron. **64**, 282011 (2021).
[46] J. M. Yao, Z. P. Li, K. Hagino, M. T. Win, Y. Y. Zhang, and J. Meng, Nucl. Phys. A **868–869**, 12 (2011).
[47] M. Isaka and M. Kimura, Phys. Rev. C **92**, 044326 (2015).
[48] E. Hiyama, M. Kamimura, Y. Yamamoto, and T. Motoba, Phys. Rev. Lett. **104**, 212502 (2010).
[49] C. Y. Song and J. M. Yao, Chin. Phys. C **34**, 1425 (2010).
[50] T. T. Sun, W. L. Lu, and S. S. Zhang, Phys. Rev. C **96**, 044312 (2017).
[51] K. Brueckner, C. Levinson, and H. Mahmoud, Phys. Rev. **95**, 217 (1954).
[52] Y. Yamamoto and H. Bandō, Prog. Theor. Phys. **69**, 1312 (1983).
[53] Y. Yamamoto and Th. A. Rijken, Nucl. Phys. A **804**, 139 (2008).
[54] M. Isaka, Y. Yamamoto, and Th. A. Rijken, Phys. Rev. C **95**, 044308 (2017).
[55] M. M. Nagels, Th. A. Rijken, and Y. Yamamoto, Phys. Rev. C **99**, 044003 (2019).
[56] M. Isaka, Y. Yamamoto, and T. Motoba, Phys. Rev. C **101**, 024301 (2020).
[57] J. Guo, X.-R. Zhou, and H. J. Schulze, Phys. Rev. C **104**, L061307 (2021).
[58] J. R. Stone and P.-G. Reinhard, Prog. Part. Nucl. Phys. **58**, 587 (2007).
[59] J. Mareš and B. K. Jennings, Phys. Rev. C **49**, 2472 (1994).
[60] Z. X. Liu, C. J. Xia, W. L. Lu, Y. X. Li, J. N. Hu, and T. T. Sun, Phys. Rev. C **98**, 024316 (2018).
[61] J. Haidenbauer and U.-G. Meißner, Phys. Lett. B **684**, 275 (2010).
[62] J.-N. Hu, Y. Zhang, and H. Shen, J. Phys. G **49**, 025104 (2022).
[63] R. Brockmann and W. Weise, Phys. Lett. B **69**, 167 (1977).
[64] W. Brückner, K. Kilian, J. Niewisch, B. Pietrzyk, B. Povh, H. G. Ritter, M. Uhrmacher, P. Birien, H. Catz, A. Chaumeaux *et al.*, Phys. Lett. B **79**, 157 (1978).
[65] S. H. Ren, T. T. Sun, and W. Zhang, Phys. Rev. C **95**, 054318 (2017).
[66] E. P. Wigner and L. Eisenbud, Phys. Rev. **72**, 29 (1947).
[67] G. M. Hale, R. E. Brown, and N. Jarmie, Phys. Rev. Lett. **59**, 763 (1987).
[68] J. Humblet, B. W. Filippone, and S. E. Koonin, Phys. Rev. C **44**, 2530 (1991).
[69] J. R. Taylor, *Scattering Theory: The Quantum Theory on Non-relativistic Collisions* (John Wiley and Sons, New York, 1972).
[70] L.-G. Cao and Z.-Y. Ma, Phys. Rev. C **66**, 024311 (2002).
[71] Z. P. Li, J. Meng, Y. Zhang, S.-G. Zhou, and L. N. Savushkin, Phys. Rev. C **81**, 034311 (2010).
[72] Z. P. Li, Y. Zhang, D. Vretenar, and J. Meng, Sci. China Phys. Mech. Astron. **53**, 773 (2010).
[73] V. I. Kukulin, V. M. Krasnopol'sky, and J. Horácek, *Theory of Resonances: Principles and Applications* (Kluwer Academic, Dordrecht, 1989).
[74] X.-D. Xu, S.-S. Zhang, A. J. Signoracci, M. S. Smith, and Z. P. Li, Phys. Rev. C **92**, 024324 (2015).
[75] A. U. Hazi and H. S. Taylor, Phys. Rev. A **1**, 1109 (1970).
[76] J. Aguilar and J. M. Combes, Commun. Math. Phys. **22**, 269 (1971).
[77] E. Balslev and J. M. Combes, Commun. Math. Phys. **22**, 280 (1971).
[78] B. Simon, Commun. Math. Phys. **27**, 1 (1972).
[79] J.-Y. Guo, X.-Z. Fang, P. Jiao, J. Wang, and B.-M. Yao, Phys. Rev. C **82**, 034318 (2010).
[80] R. J. Liotta, E. Maglione, N. Sandulescu, and T. Vertse, Phys. Lett. B **367**, 1 (1996).
[81] N. Li, M. Shi, J.-Y. Guo, Z.-M. Niu, and H. Liang, Phys. Rev. Lett. **117**, 062502 (2016).
[82] K.-M. Ding, M. Shi, J.-Y. Guo, Z.-M. Niu, and H.-Z. Liang, Phys. Rev. C **98**, 014316 (2018).
[83] M. Shi, Z.-M. Niu, and H. Liang, Phys. Rev. C **97**, 064301 (2018).
[84] X.-N. Cao, K.-M. Ding, M. Shi, Q. Liu, and J.-Y. Guo, Phys. Rev. C **102**, 044313 (2020).
[85] T. H. Heng and Y. W. Chu, Nucl. Sci. Tech. **33**, 117 (2022).
[86] P.-G. Reinhard, Rep. Prog. Phys. **52**, 439 (1989).
[87] P. Ring, Prog. Part. Nucl. Phys. **37**, 193 (1996).
[88] D. Vretenar, A. V. Afanasjev, G. A. Lalazissis, and P. Ring, Phys. Rep. **409**, 101 (2005).
[89] J. Meng, H. Toki, S. G. Zhou, S. Q. Zhang, W. H. Long, and L. S. Geng, Prog. Part. Nucl. Phys. **57**, 470 (2006).
[90] T.-T. Sun, E. Hiyama, H. Sagawa, H.-J. Schulze, and J. Meng, Phys. Rev. C **94**, 064319 (2016).
[91] S. Ajimura, H. Hayakawa, T. Kishimoto, H. Kohri, K. Matsuoka, S. Minami, T. Mori, K. Morikubo, E. Saji, A. Sakaguchi *et al.*, Phys. Rev. Lett. **86**, 4255 (2001).